

Interaction-Free Polarimetry

Jonte R. Hance^{1,*} and John Rarity¹

¹*Quantum Engineering Technology Laboratories, Department of Electrical and Electronic Engineering, University of Bristol, Woodland Road, Bristol, BS8 1US, UK*

The combination of interaction-free measurement and the quantum Zeno effect has been shown to both increase the signal-to-noise ratio of imaging, and decrease the light intensity flux through the imaged object. So far though, this has only been considered for discrimination between translucent and opaque areas of an object. In this paper, we extend this to the polarimetry of a given sample. This will allow the identification and characterisation of these samples with far less absorbed energy than current approaches—a key concern for delicate samples being probed with high-frequency radiation.

I. INTRODUCTION

Polarimetry is the task of identifying the effect a given thin sample has on the polarisation of light transmitted through that sample [1, 2]. This allows the discrimination of superficially-similar chemical samples (e.g. discriminating between different isomers, despite their identical chemical composition [3–5]). However, as polarimetry requires light flux through the sample, it can easily cause energy-related degradation—especially in samples formed of complex, photosensitive molecules. Therefore, some way of performing polarimetry with reduced (or no) photon flux through the imaged object would be a major improvement to the technique.

Interaction-free detection involves using single-particle interferometry to detect whether or not there is a block on the arm of an interferometer the particle didn't travel down. Elitzur and Vaidman initially described this phenomenon in their famous 'bomb detector thought experiment', where there is a chance to see whether a potentially faulty bomb works without detonating it [6]. Kwiat et al then refined this using the Quantum Zeno effect, to reduce the chance of the particle going down the arm with the blocker (or bomb) to effectively zero [7].

However, while this phenomena has been developed to great effect for both classical [8–10] and quantum [11–13] communication, so far interaction-free measurement has only been deployed to image the presence/absence (or opacity/transparency) of an object [14–19]. In this paper, we extend this powerful tool to the detection of polarising effects in a given sample. We do this while still maintaining the key benefits of the interaction-free/quantum Zeno coupled approach—low photon flux/energy absorption by the object being imaged.

II. DEFINING POLARIMETRY

Classically, we treat a polarised monochromatic light wave travelling in direction \mathbf{k} as

$$\mathbf{E}(\mathbf{r}, t) = (h\hat{\mathbf{h}} + v\hat{\mathbf{v}})e^{i\mathbf{k}\cdot\mathbf{r} - i\omega t} \quad (1)$$

where h and v are complex constants, and $\hat{\mathbf{h}}$ and $\hat{\mathbf{v}}$ are unit vectors orthogonal to both each other and \mathbf{k} . We categorise the polarisation properties of this wave \mathbf{E} using the Stokes parameters [2]

$$\begin{aligned} S_0 &= |\hat{\mathbf{h}} \cdot \mathbf{E}|^2 + |\hat{\mathbf{v}} \cdot \mathbf{E}|^2 = |h|^2 + |v|^2 \\ S_1 &= |\hat{\mathbf{h}} \cdot \mathbf{E}|^2 - |\hat{\mathbf{v}} \cdot \mathbf{E}|^2 = |h|^2 - |v|^2 \\ S_2 &= 2 \operatorname{Re}[(\hat{\mathbf{h}} \cdot \mathbf{E})^* \cdot (\hat{\mathbf{v}} \cdot \mathbf{E})] = h^*v + hv^* \\ S_3 &= 2 \operatorname{Im}[(\hat{\mathbf{h}} \cdot \mathbf{E})^* \cdot (\hat{\mathbf{v}} \cdot \mathbf{E})] = -i(h^*v - hv^*) \end{aligned} \quad (2)$$

Note $S_0^2 = S_1^2 + S_2^2 + S_3^2$, meaning we can define a vector $\mathbf{S} \equiv (S_1, S_2, S_3)$, which, when normalised by S_0 , spans the surface of the unit Poincaré sphere. In this way, we can associate S_1 with the H/V basis, S_2 with the D/A basis, and S_3 with the R/L basis.

When dealing with stochastic (semi-unpolarised) light, this vector \mathbf{S}/S_0 lies inside the Poincaré sphere—therefore, we can use this to give us the degree of polarisation:

$$p = |\mathbf{S}|/S_0 \quad (3)$$

All classical light rays can be decomposed into p times a perfectly polarised ray, plus $(1 - p)$ times a perfectly unpolarised ray.

Using this, we can now formally define polarimetry, as identifying how a material linearly transforms the Stokes parameters of an incoming light ray. For a given material, this transform will be by the 4×4 Mueller matrix M , where

$$S_\mu \rightarrow \sum_{\nu=0}^3 M_{\mu,\nu} S_\nu \quad (4)$$

* jonte.hance@bristol.ac.uk

Therefore, the goal of polarimetry is to identify the components of the Mueller matrix of our object. This is typically done classically by shining bright, perfectly polarised light onto the object, repeating this for different polarisation orientations (to cover the two orthogonal polarisation states of each of the three mutually unbiased bases (MUBs) for polarisation—i.e., H/V , D/A and L/R), and then using matrix inversion.

For this, we require the output Stokes parameters—thankfully, these can be obtained by summing various intensities of light output after different polarisers:

$$\begin{aligned} S_0 &= I_H + I_V \\ S_1 &= I_H - I_V \\ S_2 &= I_D - I_A \\ S_3 &= I_R - I_L \end{aligned} \quad (5)$$

where I_X is the intensity of the output beam after then being completely polarised in a given direction. Using the 36 parameters we get (6 output parameters for each of the 6 input polarisations), we can obtain the Mueller matrix for any generalised optically-transmissive medium.

In this paper, we aim to replace this bright polarised light with polarised single photons, so as to make use of interaction-free measurement and the quantum Zeno effect to reduce light incident on the object being investigated.

An arbitrary Mueller matrix for a given object can be decomposed into the product of the three generalised Mueller matrices: a retarder, a diattenuator, a the depolariser, in a unique decomposition for each given ordering of the three components (i.e. $M^d M^D M^R \neq M^R M^D M^d$). Practically, this can be viewed as any transparent object being representable as a retarder, a diattenuator, and a depolariser in some order being applied in sequence to the light ray.

A diattenuator is an object which allows light through in different proportions depending on the direction of the light's polarisation; therefore, it takes perfectly polarised light to perfectly polarised light of a different intensity, while potentially depolarising further semi-unpolarised light.

The generalised form for Mueller matrices for pure diattenuators is

$$\begin{aligned} M_D &= \tau \begin{pmatrix} 1 & \mathbf{D}^T \\ \mathbf{D} & \mathbf{m}_D \end{pmatrix}; \\ \mathbf{D} &= \begin{pmatrix} D_{H/V} \\ D_{D/A} \\ D_{R/L} \end{pmatrix}; \\ D_{MUB} &= \frac{|I_1 - I_2|}{I_1 + I_2} \\ \mathbf{m}_D &= \sqrt{1 - |\mathbf{D}|^2} \mathbb{1}_3 + \left(1 - \sqrt{1 - |\mathbf{D}|^2}\right) \mathbf{D} \mathbf{D}^T \end{aligned} \quad (6)$$

where I_1 and I_2 are the intensities measured from the two

orthogonal input polarisation states of the input MUB.

In this paper, due to the limitations of interaction-free probing, we focus on the polarimetry of diattenuating samples.

III. PROTOCOL

To achieve interaction-free polarimetry, we start with an apparatus similar to that used to counterfactually ghost image objects in [18]. However, it is arranged both to allow the probing of an object with different polarisations of light, and so the high-resolution intensified charge-coupled device (ICCD) cameras receive the photon from the interaction-free measurement protocol directly, with what was the ghost-path in [18] now being used for polarisation-based heralding. We give an apparatus for this in Fig.1.

In this protocol, we use a polarisation and position-momentum entangled pair of photons, split at our $\pi/4$ (50:50) beamsplitter. We send one photon to our chained multi-pixel Michelson interferometer array, with the object to be imaged in one path (the imaging photon). We send the other photon goes to our variable polarising beamsplitter (PBS), where we can choose a polarisation basis to image the object in (the heralding photon).

On exiting the $\pi/4$ beamsplitter, the imaging photon enters a multi-pixel version of the chained interaction-free measurement device, designed to maintain pixel coherence. Here, it enters a $\pi/4n$ beamsplitter, where we define a θ beamsplitter as performing a Pauli-Y rotation between two path modes of rotation angle 2θ :

$$\hat{\mathbf{R}}_y(2\theta) = \begin{pmatrix} \cos(\theta) & -\sin(\theta) \\ \sin(\theta) & \cos(\theta) \end{pmatrix} = e^{-i\theta\hat{\sigma}_y} \quad (7)$$

This sends some probability amplitude of the photon to the object (where it is either absorbed, or travels through it, to a mirror, back through it, and back to the beamsplitter, or some combination of the two), and some via an empty path to a mirror and back to the $\pi/4n$ beamsplitter. These two paths are the same length, to ensure no phase difference between the two components—they interfere at the beamsplitter, some parts reflecting and some transmitting, and on both transmitted and reflected path are reflected off the switchable mirrors. Therefore, these components return to again interfere at the $\pi/4n$ beamsplitter. This constitutes one cycle. After n cycles, the switchable mirrors go from reflective to transmissive, and so the photon, if not absorbed, travels to either ICCD0 or ICCD1 depending on interference.

These two outputs corresponding to the photon being blocked (ICCD1) or not blocked (ICCD0) by the object, and have variable polarisers placed in front of them, to allow us to choose a detection polarisation (H , V , D , A , R or L).

The variable-PBS (heralding) arm uses a quarter wave, then half-wave, then another quarter wave plate to rotate

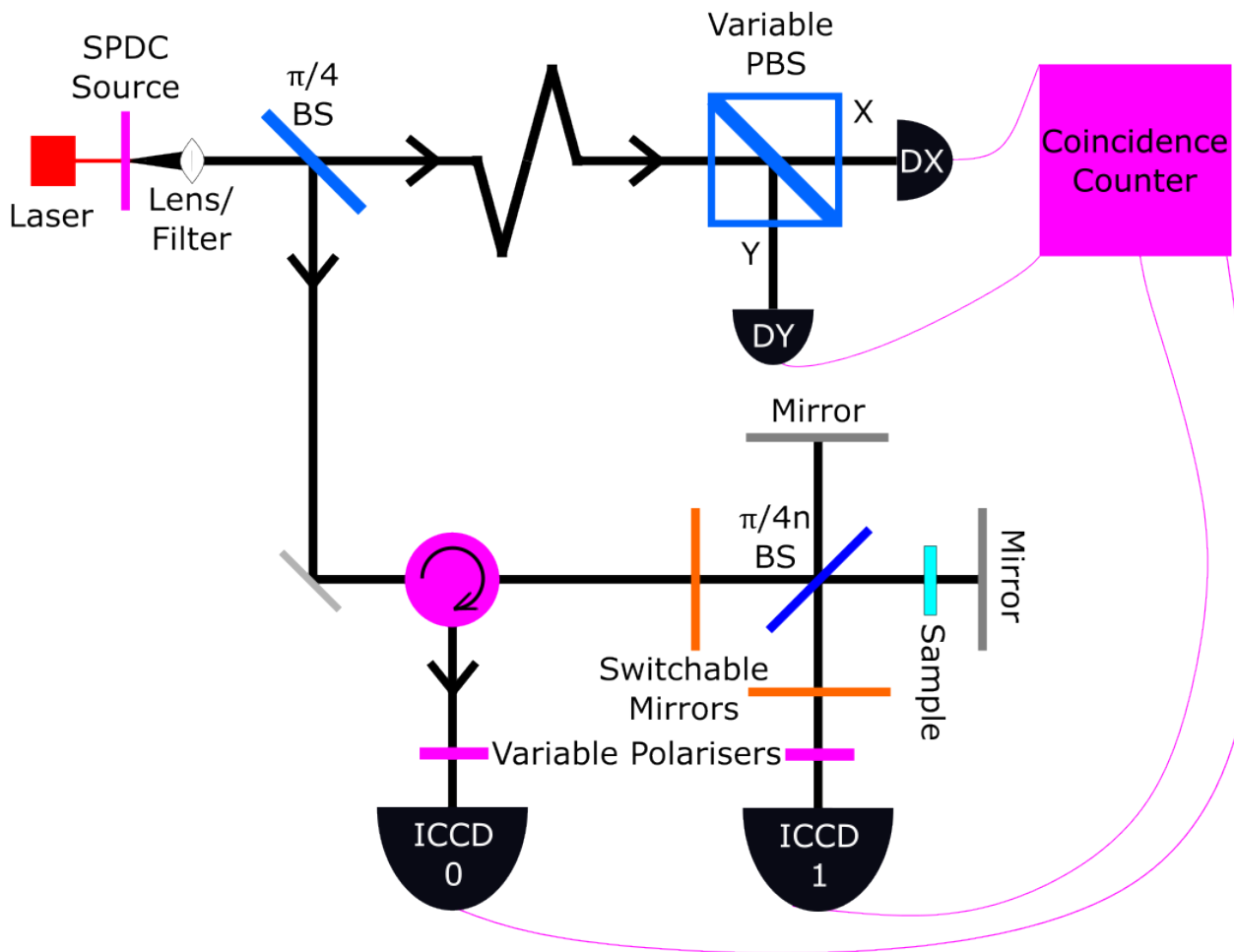


FIG. 1. Protocol for using an entangled photon pair to image a transparent, potentially polarised object, using interaction free measurement and the quantum Zeno effect to reduce photon flux on (and so energy absorbed by) the object. The variable polarising beamsplitter (PBS) allows us to pick a polarisation basis to image in (e.g. H/V , D/A , R/L), by using wave plates to rotate from that basis into the H/V basis, then applying a standard H/V polarising beamsplitter. The switchable mirrors allow the photon into the interferometer, and then keep it there for n cycles. As the number of interferometer runs n goes to infinity, the probability of the photon interacting with the transparent object goes to 0.

the photon from the imaging basis (either H/V , D/A or R/L) into the H/V basis. We then split the two orthogonal polarisations for separate detection using a normal (H/V) PBS. We record the correlations between either of the two ICCDs and either of the two polarisation-basis detectors (DX and DY). By building up correlation-based images of the object in each of the three mutually unbiased bases (MUBs) which exist for polarisation (e.g. H/V , D/A , L/R), we can slowly build up polarisation statistics for the object—allowing us to derive the Mueller matrices for each of the pixel-regions of the object.

Note, unless n goes to infinity, the protocol itself will reduce the overall intensity of light returning compared to light inserted. However, this reduction in intensity will be the same regardless of polarisation, so will not affect

the results of the protocol.

A. Imaging of Polarisation-Sensitive Metasurfaces

A useful way to prove the metrological benefits of combining polarisation-detecting protocols with interaction-free and quantum Zeno modifications, alongside pixel-mode imaging like in [18] and [19], is to show how it can be used for imaging the multiple different polarisation-dependent images that can be stored in a polarisation-sensitive metasurface. Altuzarra et al previously demonstrated polarimetry of a polarisation-sensitive metasurface using entangled pairs of photons [20], using a similar heralded polarisation-checked protocol to ours (albeit one that wasn't counterfactual). It would therefore

be interesting to perform a similar experiment using our protocol, for comparison.

IV. DISCUSSION

A. Modelling Detection/Interaction Rates

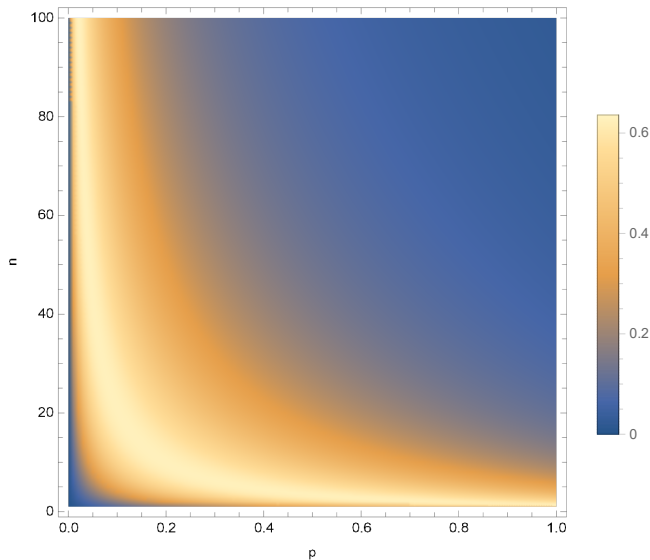


FIG. 2. Probability of the sample absorbing the probe photon in an overall run of the protocol, as a function of p , the effective probability of the object blocking that polarisation-pixel mode, and n , the number of interferometer cycles in the run.

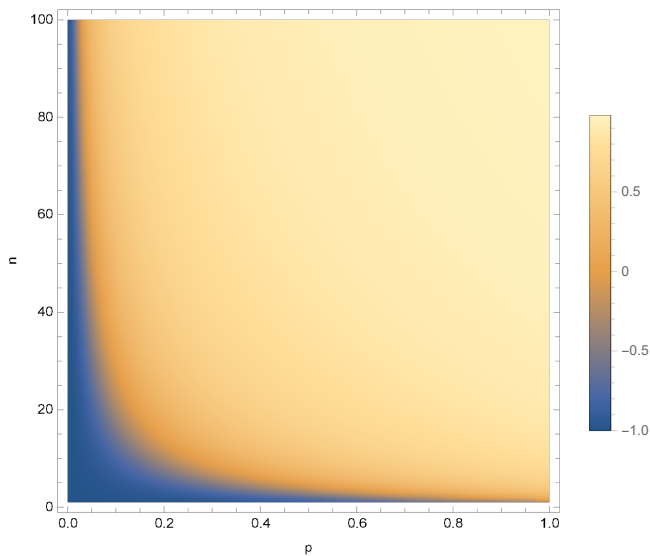


FIG. 3. Probability of the photon going to $D0$ minus the probability of it going to $D1$, as a function of p , the effective probability of the object blocking that polarisation-pixel mode, and n , the number of interferometer cycles in the run.

To evaluate the efficacy of the protocol, we need a way to describe the probability of the photon either arriving in one of the detectors, or being absorbed by the sample.

To do this, we consider a single polarisation-mode for a single pixel. We model the diattenuation of this polarisation mode for a single pass through the object probabilistically, as p times the object blocking the mode, plus $1 - p$ times the object not blocking that mode (identity). This gives us the probability of the object absorbing the photon (Fig. 2), and the probability of the photon arriving in $D0$ minus the probability of it arriving in $D1$ (Fig. 3).

As we can see from Fig 2, the probability of the photon being absorbed by the object very quickly gets far lower than what would be the case in a standard polarimetry protocol (as given by p) as we increase n .

B. Signal-to-Noise Ratio

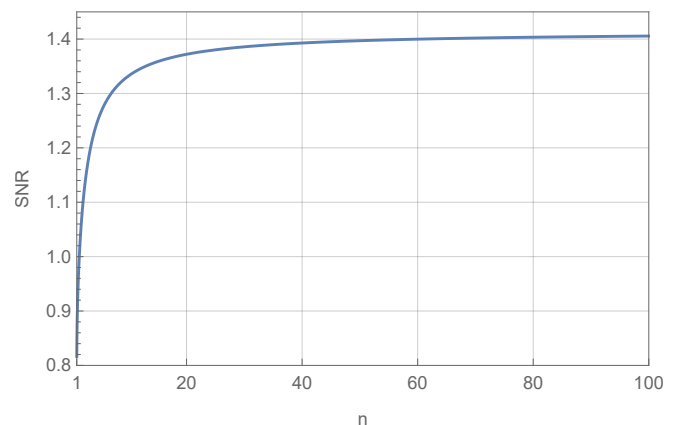


FIG. 4. SNR for each polarisation-pixel mode, normalised by dividing by $\sqrt{\bar{N}}$, the square root of the average number of photons emitted into that mode. This is a function of n , the number of interferometer cycles in the run. Given the standard SNR for polarimetry here is normalised to 1, an SNR here better than 1 indicates the protocol is better than standard polarimetry.

The signal-to-noise ratio (SNR) [21–23], a useful measure of the efficacy of an imaging system, is given by

$$\text{SNR} = \frac{|\Delta \bar{I}|}{\sigma(|\Delta \bar{I}|)} \quad (8)$$

where $\Delta \bar{I}$ is the maximal difference in average intensity values observed by a detector, and $\sigma(|\Delta \bar{I}|)$ is the standard deviation in this difference.

For standard polarimetry, an average of \bar{N} photons (those generated in a given time interval by a SPDC source) interrogate an object. This spontaneous parametric down-conversion has thermal statistics for rate of emission (which look Poissonian averaged over many temporal modes). Therefore, considering each polarisation-

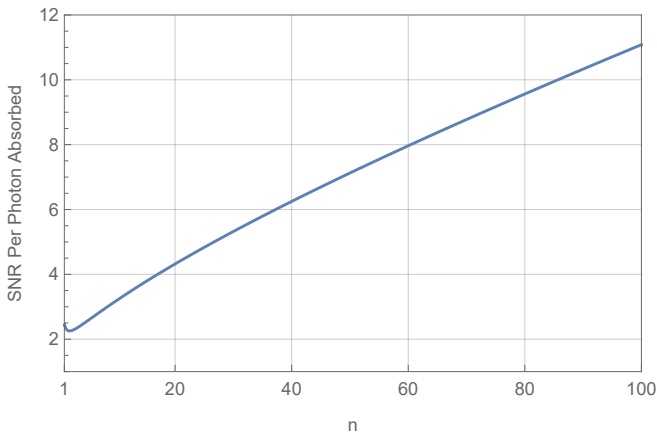


FIG. 5. SNR per photon absorbed, for each polarisation-pixel mode, normalised by dividing by $\sqrt{\bar{N}}$, the square root of the average number of photons emitted into that mode. This is a function of n , the number of interferometer cycles in the run. Given the standard SNR for polarimetry here is normalised to 1, an SNR here better than 1 indicates the protocol is better per photon absorbed than standard polarimetry.

pixel mode, if we take ΔI as the difference in number of photons arriving at our detector between when the object is maximally transmissive to that polarisation in that pixel, and when it is maximally absorptive to that polarisation in that pixel (\bar{N}), the signal to noise ratio (SNR) is

$$\text{SNR}_{\text{Pol}} = \frac{|\Delta \bar{I}|}{\sigma(|\Delta \bar{I}|)} = \frac{\bar{N}}{\sqrt{\bar{N}}} = \sqrt{\bar{N}} \quad (9)$$

For our above model, we define ΔN_{D0} (ΔN_{D1}) as the difference in photon numbers received at $D0$ ($D1$) between the object being transmissive to that polarisation in that pixel, and maximally absorptive to that polarisation in that pixel (which in each case is \bar{N} , the average number of photons emitted into that mode, times the difference in probability of a photon reaching that detector in each of those two cases). Note, ΔN_{D0} and ΔN_{D1} will have opposite signs. Therefore,

$$\begin{aligned} \text{SNR}_{\text{IFP}} &= \frac{|\Delta N_{D0} - \Delta N_{D1}|}{\sigma(|\Delta N_{D0} - \Delta N_{D1}|)} \\ &= f(n)\sqrt{\bar{N}} = f(n) \cdot \text{SNR}_{\text{Pol}} \end{aligned} \quad (10)$$

where we plot $f(n)$ in Fig. 4.

However, more relevant to us is the SNR per photon absorbed by the sample. Averaging over the number of photons interacting with the sample as a function of p and n from Fig.2, for 100 equally-spaced values of p , and dividing the SNR by the square root of that, we get the SNR per photon absorbed

$$\begin{aligned} \text{SNR}_{\text{Absd}} &= f(n)\sqrt{\bar{N}/P_{\text{Absd}}} \\ &= g(n)\sqrt{\bar{N}} = g(n) \cdot \text{SNR}_{\text{Pol}} \end{aligned} \quad (11)$$

where we plot $g(n)$ in Fig. 5.

V. CONCLUSION

In this paper, we gave an extension of counterfactual imaging to imaging of polarising objects, and then to full polarimetry of a given sample. This allows far better imaging of these samples than is currently available, with far less absorbed energy—a key concern for delicate samples being imaged with high-frequency radiation. While this protocol still needs to be formally analysed (to show the Fisher information), we can infer from the benefits previously shown for counterfactual/interaction-free based protocols, that this protocol will provide an advantage for low-energy polarimetry.

Acknowledgements— We thank ZhaoQiZhi Han for useful discussions. This work was supported by the University of York’s EPSRC DTP grant EP/R513386/1, the EPSRC Quantum Communications Hub (funded by the EPSRC grant EP/M013472/1 and EP/T001011/1), and QuantIC (the UK Quantum Technology Hub in Quantum Imaging, funded by the EPSRC grants EP/MO1326X/1 and EP/T00097X/1).

-
- [1] J Scott Tyo, Dennis L Goldstein, David B Chenault, and Joseph A Shaw. Review of passive imaging polarimetry for remote sensing applications. *Applied optics*, 45(22):5453–5469, 2006. doi:10.1364/AO.45.005453.
- [2] Aaron Z Goldberg. Quantum theory of polarimetry: From quantum operations to mueller matrices. *Physical Review Research*, 2(2):023038, 2020. doi:10.1103/PhysRevResearch.2.03038.
- [3] W Boehme, G Wagner, U Oehme, and U Priesnitz. Spec-

- trophotometric and polarimetric detectors in liquid chromatography for the determination of enantiomer ratios in complex mixtures. *Analytical Chemistry*, 54(4):709–711, 1982.
- [4] Markus D Müller, Thomas Poiger, and Hans-Rudolf Buser. Isolation and identification of the metolachlor stereoisomers using high-performance liquid chromatography, polarimetric measurements, and enantioselective gas chromatography. *Journal of agricultural and food*

- chemistry*, 49(1):42–49, 2001.
- [5] Anna K Duell, Paul J Kerber, Wentai Luo, and David H Peyton. Determination of (r)-(+)- and (s)-(-)-nicotine chirality in puff bar e-liquids by 1h nmr spectroscopy, polarimetry, and gas chromatography–mass spectrometry. *Chemical Research in Toxicology*, 34(7):1718–1720, 2021.
- [6] Avshalom C. Elitzur and Lev Vaidman. Quantum mechanical interaction-free measurements. *Found. Phys.*, 23(7):987–997, Jul 1993.
- [7] Paul Kwiat, Harald Weinfurter, Thomas Herzog, Anton Zeilinger, and Mark A. Kasevich. Interaction-free measurement. *Phys. Rev. Lett.*, 74:4763–4766, Jun 1995.
- [8] Hatim Salih, Zheng-Hong Li, Mohammad Al-Amri, and Muhammad Suhail Zubairy. Protocol for direct counterfactual quantum communication. *Phys. Rev. Lett.*, 110:170502, Apr 2013.
- [9] Hatim Salih, Will McCutcheon, Jonte R. Hance, and John Rarity. The laws of physics do not prohibit counterfactual communication. *npj Quantum Information*, 8(1):60, May 2022. doi:10.1038/s41534-022-00564-w.
- [10] Jonte R Hance, James Ladyman, and John Rarity. How quantum is quantum counterfactual communication? *Found. Phys.*, 51(1):12, Feb 2021. doi:10.1007/s10701-021-00412-5.
- [11] Hatim Salih. Protocol for counterfactually transporting an unknown qubit. *Frontiers in Physics*, 3:94, 2016.
- [12] Hatim Salih, Jonte R Hance, Will McCutcheon, Terry Rudolph, and John Rarity. Exchange-free computation on an unknown qubit at a distance. *New J. Phys.*, 23(1):013004, jan 2021. doi:10.1088/1367-2630/abd3c4.
- [13] Hatim Salih, Jonte R. Hance, Will McCutcheon, Terry Rudolph, and John Rarity. Deterministic teleportation and universal computation without particle exchange. *arXiv preprint arXiv:2009.05564*, 2020. URL: <https://arxiv.org/abs/2009.05564>.
- [14] Andrew G. White, Jay R. Mitchell, Olaf Nairz, and Paul G. Kwiat. “interaction-free” imaging. *Phys. Rev. A*, 58:605–613, Jul 1998.
- [15] Jean-Pierre Wolf and Yaron Silberberg. Spooky spectroscopy. *Nature Photonics*, 10(2):77–79, 2016. doi:10.1038/nphoton.2015.267.
- [16] Yingwen Zhang, Alicia Sit, Frédéric Bouchard, Hugo Larocque, Florence Grenapin, Eliahu Cohen, Avshalom C Elitzur, James L Harden, Robert W Boyd, and Ebrahim Karimi. Interaction-free ghost-imaging of structured objects. *Opt. Express*, 27(3):2212–2224, 2019.
- [17] Yu Chen, Yu-Jie Cai, Xing-Tong Li, Kun Huang, Jin-Ming Liu, and E Wu. Interaction-free quantum spectroscopy. *Advanced Photonics Research*, page 2000206, 2021. doi:10.1002/adpr.202000206.
- [18] Jonte R Hance and John Rarity. Counterfactual ghost imaging. *npj Quantum Information*, 7(1):1–7, 2021. doi:10.1038/s41534-021-00411-4.
- [19] Alexandra Maria Pălici, Tudor-Alexandru Isdrailă, Stefan Ataman, and Radu Ionicioiu. Interaction-free imaging of multipixel objects. *Phys. Rev. A*, 105:013529, Jan 2022. doi:10.1103/PhysRevA.105.013529.
- [20] Charles Altuzarra, Ashley Lyons, Guanghui Yuan, Christy Simpson, Thomas Roger, Jonathan S Ben-Benjamin, and Daniele Faccio. Imaging of polarization-sensitive metasurfaces with quantum entanglement. *Physical Review A*, 99(2):020101, 2019. doi:10.1103/PhysRevA.99.020101.
- [21] Malcolm N. O’Sullivan, Kam Wai Clifford Chan, and Robert W. Boyd. Comparison of the signal-to-noise characteristics of quantum versus thermal ghost imaging. *Phys. Rev. A*, 82:053803, Nov 2010.
- [22] G. Brida, M. V. Chekhova, G. A. Fornaro, M. Genovese, E. D. Lopaeva, and I. Ruo Berchera. Systematic analysis of signal-to-noise ratio in bipartite ghost imaging with classical and quantum light. *Phys. Rev. A*, 83:063807, Jun 2011.
- [23] Marco Genovese. Real applications of quantum imaging. *J. Opt. UK*, 18(7):073002, jun 2016.